ADVANCING EARTH AND SPACE SCIENCE

JGR Solid Earth

RESEARCH ARTICLE
10.1029/2020JB020628

Key Points:

- Far-regional displacements for a great earthquake are dominated by permanent displacement, elastogravity waves, and long-period waves
- Density disturbance in the great earthquake source region produces elastogravity waves instantly on earthquake occurrence
- A great earthquake produces strong ground displacements with minimal ground accelerations at far-regional distances

Supporting Information:

- Supporting Information S1

Correspondence to:
T.-K. Hong,
tkhong@yonsei.ac.kr

Citation:
Hong, T.-K., Kim, I., Park, S., & Kil, D. (2021). Elastogravity waves and dynamic ground motions in the Korean Peninsula generated by the March 11, 2011 M_W9.0 Tohoku-Oki megathrust earthquake. *Journal of Geophysical Research: Solid Earth*, *126*, e2020JB020628. https://doi.org/10.1029/2020JB020628

Received 17 JUL 2020
Accepted 5 DEC 2020

Elastogravity Waves and Dynamic Ground Motions in the Korean Peninsula Generated by the March 11, 2011 M_W9.0 Tohoku-Oki Megathrust Earthquake

Tae-Kyung Hong[1], Ilgoo Kim[1], Seongjun Park[1], and Dongwoo Kil[1]

[1]Department of Earth System Sciences, Yonsei University, Seoul, South Korea

Abstract The mass dislocations caused by large coseismic slips in megathrust earthquakes are large enough to produce elastogravity waves. Despite, successful identification of elastogravity-wave development during megathrust earthquakes, the nature of ground motions and hazard potentials in regional and teleseismic distances remains unknown. The dynamic ground motions from the March 11, 2011 M_W9.0 Tohoku-Oki megathrust earthquake are retrieved from broadband seismic records throughout the Korean Peninsula. The dynamic ground motions of the megathrust earthquake are dominated by low-frequency (<0.1 Hz) energy that is a mixture of elastogravity waves and seismic waves. The peak dynamic ground displacements in the Korean Peninsula reached ~20 cm with horizontal permanent displacements of ~2 cm or more. Radially-polarized elastogravity waves developed instantly at the event origin time. Very-long-period (<0.004 Hz) energy is a mixture of seismic waves and coseismic permanent displacements, presenting radially polarized retrograde particle motions for ~600 s. The peak ground displacements (PGDs) and velocities for the Tohoku-Oki earthquake are larger than those for a local M_W5.4 earthquake. The peak ground motions vary azimuthally following the source radiation pattern. The tangential PGD increases with distance along continental ray paths due to the development of crustally guided waves. Large and slow dynamic ground motions cause dynamic stress changes of ~1.8 MPa in the lithosphere of the Korean Peninsula, while the properties of the mantle are scarcely affected by slow dynamic motions. The large long-period displacements induced by megathrust earthquakes may cause considerable long-duration distortion on large buildings at regional and teleseismic distances. The characteristic elastogravity-wave features may be used for detection of mass-dislocation events.

Plain Language Summary The long source durations of great earthquakes produce predominantly long-period waves that survive with large amplitudes over long distances. The slow dynamic deformation of subsurface media and the seismic hazard potentials pertaining to long-period waves have received relatively little attention. This study, investigates the properties of the dynamic ground motions at far-regional distances produced by the March 11, 2011 M_W9.0 Tohoku-Oki megathrust earthquake. We retrieve the dynamic ground motions in the full frequency range from broadband seismic records, presenting the elastogravity waves, strong long-period seismic waves and coseismic permanent displacements. Elastogravity waves develop promptly at the event origin time due to density disturbances in the source region. Large PGDs and peak ground velocities occurred at far-regional distances as a result of this megathrust earthquake. The dynamic ground motions are characterized by azimuth- and distance-dependent features, which may be crucial for seismic design and seismic hazard mitigation for regional megathrust earthquakes.

1. Introduction

A large earthquake produces strong ground motions that are a combination of permanent and transient displacements. These ground motions originate from fault slip and gravity perturbations. Permanent ground displacements decay exponentially with distance. A megathrust earthquake may produce coseismic permanent displacements on the order of several millimeters thousands of kilometers away (Shestakov et al., 2012; M. Wang, Li, et al., 2011).

The dislocation of a mass during a megathrust earthquake causes a gravity perturbation in the source region (Vallée et al., 2017). These gravity perturbations excite elastogravity waves that propagate radially at the speed of light. The elastogravity waves can be identified before the arrival times of *P* waves in very-long-period record sections (Harms et al., 2015; Montagner et al., 2016). The elastogravity waves are naturally mixed with transient seismic waves due to inherent long duration by fast propagation around the Earth with low attenuation. The nature and influences of the elastogravity waves are poorly known. Further the nature and influences of the elastogravity waves are poorly known.

Dynamic ground motions induce stress changes that may trigger earthquakes (Gomberg et al., 2001; D. P. Hill et al., 1993; Hill & Prejean, 2007; Houng et al., 2016). In this mechanism, a dynamic stress change decreases the Young's modulus of the surrounding medium, effectively triggering a seismic event (Johnson & Jia, 2005). Additionally, coseismic permanent displacements perturb the static stress field, possibly triggering earthquakes near the source region (Caskey & Wesnousky, 1997; Hong et al., 2018; Parsons et al., 2006; Reasenberg & Simpson, 1992). It was reported that the seismic velocities in the crust were changed at local and regional distances after a megathrust earthquake (Hong, Lee, Chi, et al., 2017; Kim & Hong, 2018; Nakahara, 2015; Nakata, 2011; Takagi & Okada, 2012). These crustal seismic velocity changes may be associated with stress changes and perturbations of the surrounding media (Birch, 1960; Nur & Simmons, 1969; Pei et al., 2019).

Ascertaining the intensities of strong ground motions constitutes a primary interest of research on earthquake-resistant design for the mitigation of seismic hazards. Concerns have risen regarding the increased construction of high-rize buildings in urban areas that are vulnerable to long-period (1–10 s) ground motions (Heaton et al., 1995; Kanamori, 1979; Koketsu & Miyake, 2008; Kukuwa & Tobita, 2008). Buildings resonate with ground motions occurring at the natural frequencies of the buildings. It was previously suggested that the natural frequency of a building follows a particular relationship (Ellis, 1980; Rossmann et al., 2015):

$$f_n = \frac{46}{H}, \tag{1}$$

where f_n is the natural frequency in Hz and H is the building height in m. Modern high-rize buildings reach heights in excess of ~800 m with natural frequencies of ~0.0575 Hz (Burj Khalifa, Dubai: 828 m and 160 stories). The heights of such buildings increase with advancing technology, and the corresponding natural frequencies decrease.

Seismic damage may be dependent on the peak ground acceleration (PGA) and peak ground velocity (PGV; Atkinson & Sonley, 2000; Dangkua & Cramer, 2011; Yaghmaei-Sabegh et al., 2011). The magnitudes of the PGA and PGV are dependent on the distances and frequency contents of source time functions. Megathrust earthquakes produce very-long-period waves. However, the contribution of very-long-period waves on the peak ground motions and potential seismic hazards has been rarely reported. Also, the influence of very-long-period dynamic ground motions on the perturbations of media and stress fields are poorly understood.

The March 11, 2011 M_W9.0 Tohoku-Oki megathrust earthquake provides a unique opportunity to examine very-long-period ground motions at large distances from the event location. The Korean Peninsula is situated in an intraplate environment at a far-regional distance from this megathrust earthquake and is equipped with a dense seismic network. Both coseismic permanent displacements and transient seismic waves were well recorded throughout the region. In this study, we investigate the coseismic ground motions generated in the Korean Peninsula by this earthquake using broadband seismic records. We determine the occurrence times of permanent displacements and of transient long-period waves containing the elastogravity and seismic waves. The estimated coseismic permanent displacements are with geodetic observations. We then investigate the influence of dynamic and static displacements on the media. We examine the three-component waveform features of elastogravity waves, which can be used for detection of small mass-dislocation events.

2. Event and Data

The March 11, 2011 M_W9.0 Tohoku-Oki megathrust earthquake occurred on the boundary between the Pacific plate and Okhotsk plate off the eastern coast of the Japanese archipelago (Figure 1). The earthquake produced a fault rupture spanning ~440 km by ~180 km with a peak slip of ~60 m (Lay et al., 2011;

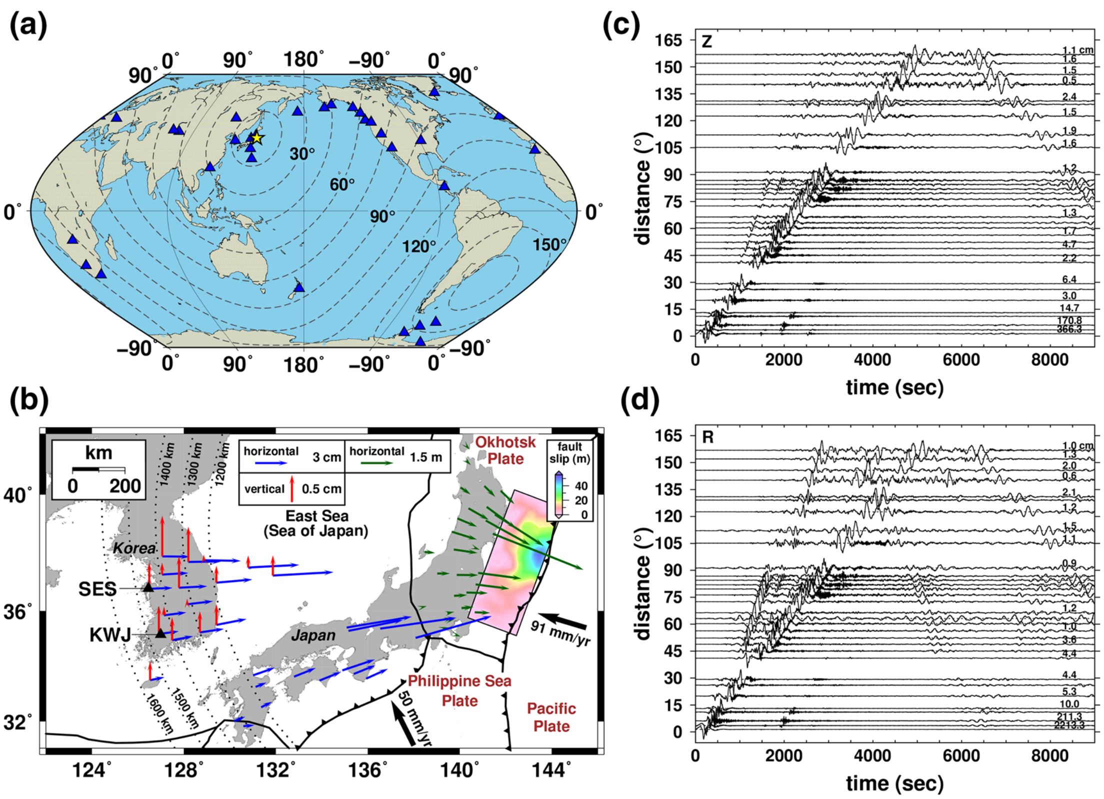

Figure 1. The March 11, 2011 M_W9.0 Tohoku-Oki megathrust earthquake and seismic waveforms: (a) map of the event and stations, (b) coseismic permanent displacements in the Korean Peninsula and Japanese islands (Baek et al., 2012; Gautam et al., 2019), and displacement seismic records on the (c) vertical (Z), and (d) radial (R) components. The seismic records are bandpass filtered in the frequency range of 0.004–8.0 Hz. Strong low-frequency seismic records are observed over the globe. The horizontal coseismic displacements are directed toward the source region. A coseismic slip model of the earthquake is presented (Yagi & Fukahata, 2011).

Suzuki et al., 2011). The slab dips at an angle of ~10° (Yagi & Fukahata, 2011). The moment rate function of the megathrust earthquake suggests a fault rupture with a duration of ~200 s (Wei et al., 2012; Yagi & Fukahata, 2011).

The megathrust earthquake generated strong ground motions as large as ~2,000 cm/s^2 to the east of the Japanese islands near the epicenter (Nakahara, 2015). Additionally, the megathrust earthquake produced strong low-frequency energy that was persistently observed at regional and teleseismic distances (Shestakov et al., 2012; M. Wang, Li, et al., 2011; Figure 1; Text S1). The peak ground displacements (PGDs) reached ~1 cm around the antipodal locations.

Discrete successive ruptures occurred during the Tohoku-Oki megathrust earthquake (Lay et al., 2011; Tajima et al., 2013). The permanent displacements reached a few meters off the eastern coast of Japan where the permanent displacements were dominant over the transient displacements (Gautam et al., 2019; Psimoulis, 2014, 2018; Suzuki et al., 2011). The Korean Peninsula is located ~1,200–1,600 km from the megathrust earthquake. Coseismic horizontal displacements of 1–5 cm were recorded in the Korean Peninsula (Baek et al., 2012; Hong et al., 2015). These coseismic displacements are comparable to the one-year relative plate motion of the Korean Peninsula relative to the Japan Trench, which suggests rapid coseismic deformation over the course of a single day. These coseismic displacements accompanied a seismic velocity reduction in the crust reaching 3% (Hong, Lee, Chi, et al., 2017). Also, there were many studies to report seismic velocity changes in the crust of Japanese islands (Kim & Hong, 2018; Nakahara, 2015; Nakata, 2011; Takagi & Okada, 2012).

We analyze the seismic records from 22 broadband velocity seismometers and 101 accelerometers. The sampling rates are 80–100 Hz. We use only the unclipped records to retrieve the coseismic displacements in full

10.1029/2020JB020628

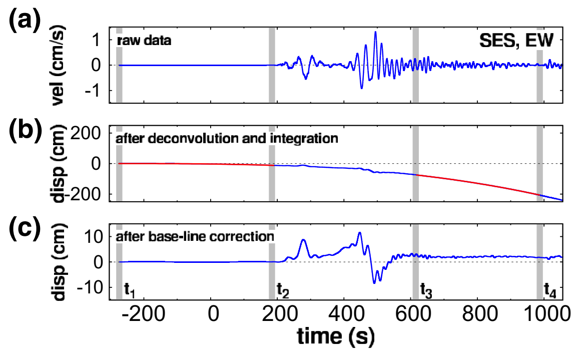

Figure 2. Procedure employed to recover the dynamic ground motions from seismic records: (a) raw velocity record section from broadband velocity station SES, (b) displacement records after deconvolution of the instrumental response and time-domain integration, and (c) displacement records after a curvilinear-drift correction. Record section are presented with blue lines. The curvilinear drifts in the time windows t_1-t_2 and t_3-t_4 are well represented by 4th-order polynomial functions (red lines).

frequency range produced by the Tohoku-Oki megathrust earthquake. We find two broadband stations with unclipped records in the western peninsula (stations SES and KWJ; Figure 1c). The epicentral distance of both stations is approximately 1,450 km. We find that the broadband velocity record in the eastern and central parts of the Korean Peninsula were clipped. On the other hand, all the accelerometers provide unclipped seismic records. The lower cut-off frequency of the broadband sensor is 0.008333 Hz, and the dynamic range of the broadband sensor is 1.3 cm/s. We use the seismic data from accelerometers for analysis of peak ground motions.

The September 12, 2016 M_L5.8 (M_W5.4) Gyeongju earthquake is the largest earthquake since 1978 when the national seismic monitoring began (Hong, Lee, Kim, et al., 2017, 2018). The Gyeongju earthquake produced significant seismic damage in local regions (Hong, Lee, Kim, et al., 2017). The Gyeongju earthquake may provide references for the levels and properties of ground motions for a local moderate-size earthquake relative to those of the far-regional megathrust earthquake. We collect the seismic records of 196 accelerometers for the Gyeongju earthquake to compare the peak ground motions with those of the Tohoku-Oki earthquake.

3. Method

The time histories of the coseismic displacements can be recovered from high-sampling-rate (>1 Hz) geodetic measurements (Baek et al., 2012; Guo et al., 2013). However, such high-sampling geodetic data are only available for some regions. Various attempts to estimate permanent displacements using accelerograms or velocity seismograms have been reported (Boore, 2001; Iwan et al., 1985; Pino & Di Luccio, 2005; R. Wang, Schurr, et al., 2011; Zhu, 2003). Strong motion records (accelerograms) are useful for recovering the displacements around source regions (Boore, 2001; Iwan et al., 1985).

We recover dynamic ground motions using unclipped broadband velocity seismograms using a time-domain integration method (Pino & Di Luccio, 2005; Zhu, 2003;). We correct the instrument response using a time-domain deconvolution method to restore the low-frequency ground motions (Anderson & Lees, 2014; Haney et al., 2012; Scherbaum, 2007; Figure 2). The recorded seismic waveform, $Y(s)$, can be written as (Anderson & Lees, 2014; Haney et al., 2012)

$$Y(s) = GT(s)X(s), \tag{2}$$

where $s = i2\pi f$, f is the frequency, G is the sensitivity, $T(s)$ is the instrument response function, and $X(s)$ represents the ground motion. Here, the complex variable s can be rewritten using a bilinear Z transform:

$$s = \frac{2}{\delta t}\left(\frac{1 - Z^{-1}}{1 + Z^{-1}}\right), \tag{3}$$

where δt is the sampling interval.

The instrument response function is approximated using a Z transform. The Z-transformed seismic waveforms are given by

$$Y(Z) = C\left\{\frac{\sum_i a_i Z^{-i}}{\sum_i b_i Z^{-i}}\right\}X(Z), \tag{4}$$

where C is the calibrated sensitivity of the Z-transformed instrument response function and a_i and b_i are constants for the poles and zeros of the instrument response. An inverse Z transform of Equation 4 yields

10.1029/2020JB020628

$$x_n = \frac{b_0}{Ca_0} y_n + \sum_{K}^{i=1} \left(\frac{b_i}{Ca_0} y_{n-i} - \frac{a_i}{a_0} x_{n-i} \right), \tag{5}$$

where x_n represents the ground motion at the nth discrete time point and y_n is the seismic record. We apply a two-pole Butterworth low-pass filter with a corner frequency of 8 Hz to avoid signal distortion around the Nyquist frequency (Haney et al., 2012).

We integrate the ground velocity records using a time-domain trapezoidal integration method, yielding ground displacement records (Figure 2). Curvilinear drift in the displacement records is corrected using fourth-order polynomial regression, which yields the dynamic ground motions in the full frequency range (Lee et al., 2002; Pino & Di Luccio, 2005; Zhu, 2003). The fourth-order polynomial regression curves effectively represent the curvilinear displacement records (Figure 2).

Transient seismic energy causes dynamic strain and stress changes in the media. The peak dynamic shear strain ϵ_m induced by dominant shear waves is given by (Hill & Prejean, 2007; Houng et al., 2016)

$$\epsilon_m = \frac{\dot{U}_m}{V_s}, \tag{6}$$

where $\dot{U}_m$ is the PGV, and V_s is the shear wave velocity. Also, the peak dynamic stress change, σ_m, is

$$\sigma_m = \mu \frac{\dot{U}_m}{V_s}, \tag{7}$$

where μ is the shear modulus.

We measure the seismic velocity changes along interstation paths using noise cross-correlation functions (Bensen et al., 2007; Campillo & Paul, 2003; Hong, Lee, Chi, et al., 2017; Shapiro et al., 2005). We stack one-bit normalized seismic noise functions to retrieve the Green's function for the interstation path. The reference noise cross-correlation function was computed from noise records spanning 213 days from June 1, 2010 to December 31, 2010.

4. Dynamic Ground Motions

We prepare the broadband velocity seismograms at stations SES and KWJ. The record sections are low-pass filtered below 8.0 Hz with correction of signal amplification in sensors and recorders (Figure 2a). We apply the time-domain integration method with instrumental response correction to the low-pass filtered record sections (Figure 2b). We obtain the coseismic ground motions in frequencies ≤ 8.0 Hz after base-line correction of the time-domain-integrated records (Figure 2c). The frequency range of the dynamic ground motions covers the full frequency band of observed seismic energy at a far-regional epicentral distance (Figure 3).

We now examine the validity of the time-integration method and inverted dynamic ground motions. We apply a bandpass filter of 0.004–8.0 Hz to the inverted dynamic ground motions. We additionally prepare displacement records in 0.004–8.0 Hz from broadband velocity seismograms using a conventional signal processing method that corrects the instrumental response in the frequency domain with application of bandpass filter. Thus, we have one set of displacement records by applying a bandpass filter to the full-frequency-range dynamic ground motions. The other set of, displacement records are calculated using a conventional frequency domain process based on velocity record sections. The displacement record sections match well each other (see Text S1). The observation verifies the inverted full-frequency-range dynamic ground motion records.

The coseismic ground motions are composed of both permanent and transient displacements. The dynamic ground motions present strong transient energy after the P arrival time. The peak dynamic motions at station SES and KWJ are between 11.61 and 11.58 cm, respectively, on the radial component, between 10.83 and 14.02 cm on the tangential component, and between 15.72 and 14.09 cm on the vertical component.

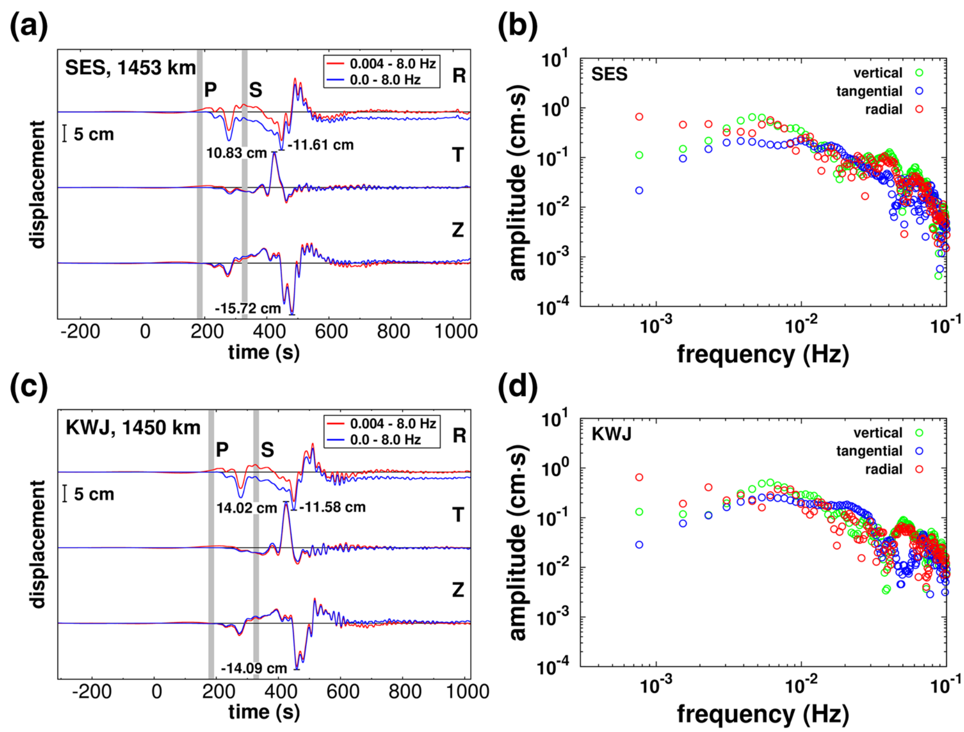

Figure 3. (a) Three-component dynamic ground motions and (b) their frequency contents at station SES, and (c), (d) those at station KWJ. Displacement record sections bandpass filtered between 0.004 and 8.0 Hz are presented for comparison. The epicentral distances and peak ground displacements are annotated. The theoretical *P* and *S* arrival times are indicated. Coseismic permanent displacements develop stably 800 s after the event origin time. Low-frequency (<0.03 Hz) energy is dominant in the ground motions for the Tohoku-Oki megathrust earthquake at far-regional distances.

The duration of dynamic ground motion spans ∼450 s. The amplitudes are comparable among the three components.

We observe constant offsets from the zero baseline in dynamic ground motions due to coseismic permanent displacements (Figure 3a). Further, the ground motions are dominated by low frequency seismic energy. The ground motions are rich in very-low-frequency energy, and the seismic energy is nearly constant at frequencies of less than 0.03 Hz (Figure 3b).

We observe ramp displacements between the arrivals of *P* waves and surface waves (Figure 3a). The ramp displacements are associated with the near-field term of displacements produced by an earthquake (Pino & Di Luccio, 2005; Zahradník & Plešinger, 2010). The feature is effectively observed in local to far-regional distances depending on the earthquake size (Pino & Di Luccio, 2005; Zahradník & Plešinger, 2010). The near-field feature is hardly observed in teleseismic records for the Tohoku-Oki earthquake (Figures 1c and 1d).

5. Coseismic Permanent Displacements

Coseismic permanent displacements generated by the March 11, 2011 M_W9.0 Tohoku-Oki megathrust earthquake were observed at local to far-regional distances (Baek et al., 2012; Gautam et al., 2019; Psimoulis, 2018; Shao et al., 2016; Suzuki et al., 2011; Figure 1). A local geodetic observation ∼75 km from the megathrust earthquake presents major displacements at two discrete moments in time (Psimoulis, 2014). The first coseismic permanent displacement of ∼2 m occurred ∼33 s after the event origin time. This time lag suggests that the apparent propagation velocity of the permanent displacement (static medium deformation) is ∼2.3 km/s. The second discrete coseismic displacement followed the first and occurred ∼73 s after the event origin time (Psimoulis, 2014). The time history of the discrete coseismic displacement is consistent with the moment rate function (Yagi & Fukahata, 2011).

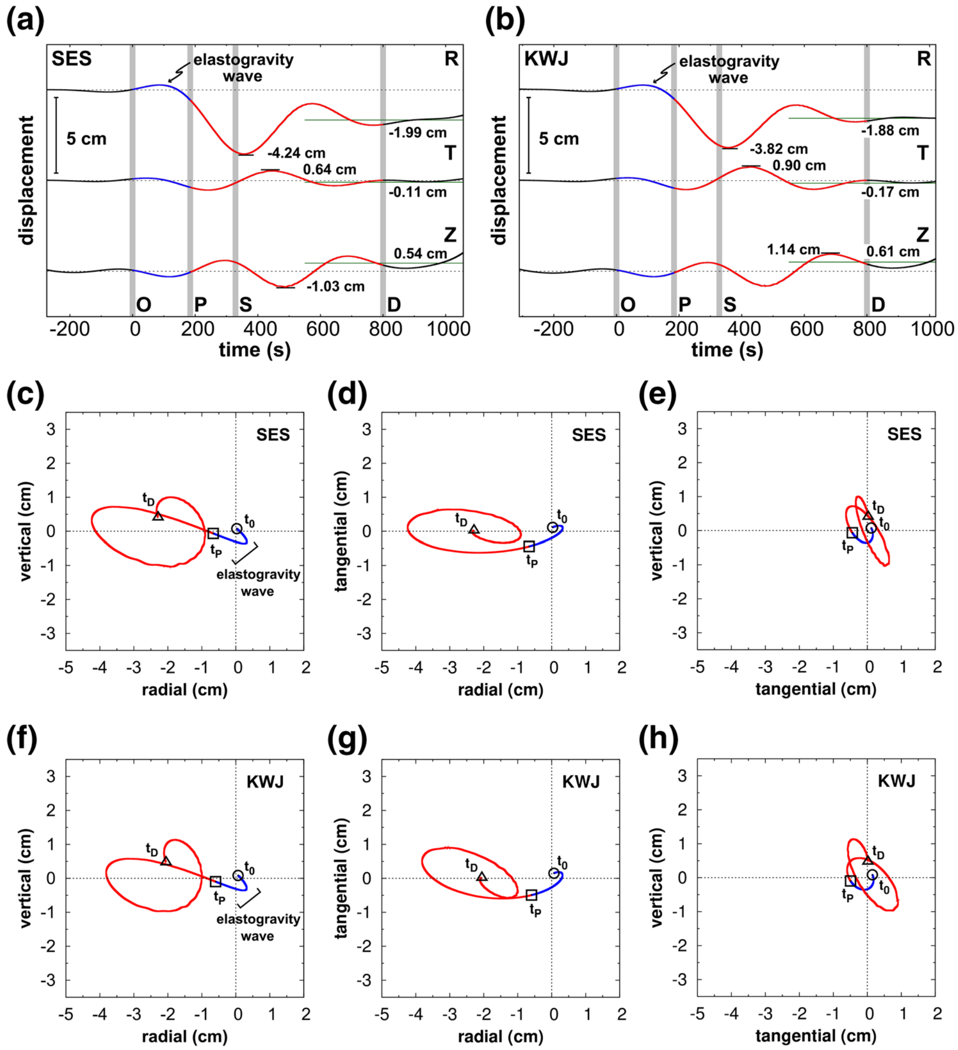

Figure 4. Very-low-frequency (<0.004 Hz) ground motions at stations (a) SES and (b) KWJ. The very-low-frequency ground motions are calculated by subtracting the bandpass filtered displacement records in 0.004–8.0 Hz from the dynamic ground motions in the full frequency range. The event origin time (O), *P* and *S* arrival times, and stable establishment times of permanent displacements (D) are marked. Elastogravity waves are observed before the *P* arrival times (blue lines). The levels of permanent displacements are annotated. Particle motions of the very-low-frequency ground motions on (c) the radial-vertical plane, (d) radial-tangential plane, (e) tangential-vertical plane from the event origin time (t_O) to the stable permanent displacement onset time (t_D) at station SES, and (f, g, and h) those at KWJ. The elastogravity waves before the *P* arrival times (t_P) present radially prograde motions. The very-long-period waves after the *P* arrival times display radially retrograde motions (red lines).

We prepare very-long-period (<0.004 Hz) ground motions at stations SES and KWJ to identify the permanent displacements. We calculate the very-long-period record sections by subtracting the displacement records at frequencies of 0.004–8.0 Hz from the full-frequency-range displacement records (Figures 4a and 4b). The wavetrains swing around the mean baselines. We find apparent mean-baseline changes in lapse times of ~620 s after the event origin time. The mean-baseline offsets from the zero-baseline suggest the magnitudes of permanent displacements (Figures 4a and 4b). The lapse times of mean-baseline changes suggest the onset times of coseismic permanent displacements (coseismic static deformation). The mean-baseline offsets at stations SES and KWJ were stabilized in lapse times of ~800 s after the event origin time.

The coseismic permanent displacements on the radial component at stations SES and KWJ are between −1.99 and −1.88 cm, respectively, while the permanent displacements on the tangential component are −0.11 and −0.17 cm, and those on the vertical component are 0.54 and 0.61 cm. The observed permanent

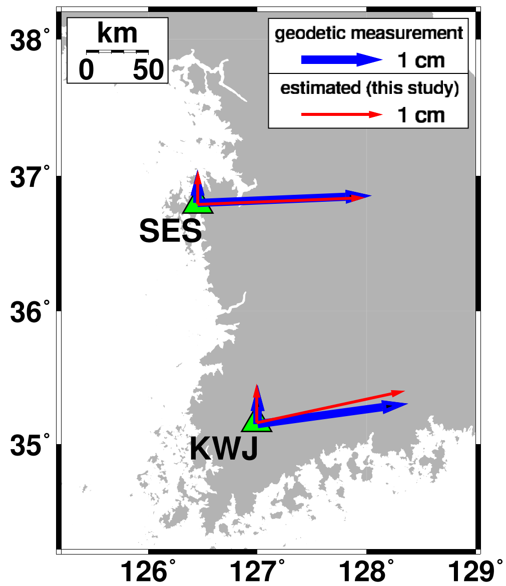

Figure 5. Amplitudes and directions of the permanent displacements inverted from the seismic records at two stations (SES and KWJ). The inverted displacements are consistent with geodetic measurements.

displacements agree with the geodetic measurements during the day (Baek et al., 2012; Hong et al., 2015; Kim et al., 2016; Kim & Hong, 2018; Zhao et al., 2012; Figure 5). The directions of the lateral coseismic permanent displacements are subparallel to the orientations of the great-circle paths between the event epicenter and stations. Also, the apparent propagation velocity of permanent displacement inferred from the apparent arrival times is consistent with geodetic field observations where the apparent propagation velocity was determined by ~2.3 km/s (Psimoulis, 2014).

These observations support the correct retrieval of coseismic permanent displacements from dynamic ground motion records. Also, we find that the very-long-period dynamic displacements are mixtures of transient motions and permanent displacements. The coseismic permanent displacements may follow the fastest transient waves and may stabilize after the arrivals of surface waves (Figures 3 and 4).

5.1. Very-Long-Period Waves

Very-long-period seismic waves can be regarded as the superposition of normal modes (or of free oscillations of the Earth). Successive seismic phases arrive following the fastest phase, *P* wave. We observe the presence of seismic energy before the *P* wave. The energy develops since the event origin time (Figures 4a and 4b). The particle motions of the energy are different from those of *P* waves (Figures 4c and 4d). Further, the seismic energy is dominant at frequencies < 0.03 Hz (Figure 3). The apparent strong energy around the event origin time is observed only in the low frequency range, which cannot be produced by filtering effect of weaker high-frequency energy. This energy corresponds to elastogravity waves (Matsuo & Heki, 2011; Montagner et al., 2016).

Elastogravity waves develop due to gravity perturbations resulting from the dislocation of a mass during a great earthquake, and these waves propagate at the speed of light (Vallée et al., 2017). Thus, elastogravity waves develop promptly at the origin time of an earthquake at far-regional distances. This gravity perturbation during the Tohoku-Oki earthquake is supported by other studies (Matsuo & Heki, 2011; Montagner et al., 2016). Vallée et al. (2017) identified the elastogravity phase from an analysis of accelerograms at low frequencies ranging from 0.002 to 0.03 Hz. The elastogravity phase determined from accelerograms is hardly apparent at the event origin time and develops rapidly with time. The acceleration phase endures for ~100 s (Vallée et al., 2017).

We observe the elastogravity waves in the very-long-period (<0.004 Hz) displacement record sections (Figures 4a and 4b). The energy before the *P* arrival time is composed entirely of elastogravity waves. These elastogravity waves are observed mainly on the radial and vertical components. The amplitudes on the radial component are comparable to those on the vertical component. On the other hand, elastogravity waves are relatively weak on the tangential component. This observation is consistent with the theoretical expression that gravity perturbations produce mainly longitudinal (compressional) waves and no shear waves (Harms et al., 2015).

The particle motions of the elastogravity waves on the radial-vertical plane present prograde motions (Figures 4c and 4d), while the particle motions on the horizontal (radial-tangential) plane display strong polarization in the radial direction. The particle motions are different from those of typical body waves and surface waves. The *P* waves present linear particle motions on the radial-vertical plane. The Rayleigh waves display vertically-elliptical retrograde particle motions polarized on the radial-vertical plane. The Love waves are polarized in the tangential direction. Theoretical particle motions present a dilatational particle motion polarized in the radial-vertical plane (Harms et al., 2015; Vallée et al., 2017). Shear energy is coupled at the free surface that may produces fractional tangential-component waves depending on the

10.1029/2020JB020628

surface topography (Vallée et al., 2017). The observed particle motions of the elastogravity waves agree with the theoretical particle motions.

The very-long-period waves after the *P* arrival times may be mixtures of transient seismic waves (normal modes) and elastogravity waves. The very-long-period waves after the *P* arrival times on the radial component of stations SES and KWJ have peak amplitudes of −4.24 and −3.82 cm, respectively (Figure 4), while the peak amplitudes on the tangential component are 0.64 and 0.90 cm, and those on the vertical component are −1.03 and 1.14 cm. The amplitudes on the radial component are much larger than those on the vertical and tangential components.

The very-long-period waves continued for ∼800 s after the event origin time, which is approximately four times the duration of the moment rate function (∼200 s) (Figures 4a and 4b). The particle motions of the very-long-period waves after the *P* arrival times present retrograde, radially-polarized, and laterally elongated motions on the radial-vertical plane (Figures 4c and 4d). The particle motions on the horizontal (radial-tangential) plane present polarization in the radial direction. These observations suggest that the very-long-period waves mainly propagated radially from the source region.

It is worth noting that the orientations of particle motions on the radial-vertical planes are different before and after the *P* arrival times. The prograde particle motions before the *P* arrival times change to retrograde motions after the *P* arrival times. These different particle motions support a difference in the constituent energy. The wavetrains before the *P* arrival times are composed of elastogravity waves, while those after the *P* arrival times are a mix of elastogravity waves, transient seismic phases and coseismic permanent displacements.

6. Frequency Contents

The transient seismic waves composing the high-frequency component decay rapidly with distance. Thus, the frequency contents of the dynamic ground motions at far-regional distances are mainly composed of low-frequency energy. The dominant energy is observed at frequencies of less than 0.03 Hz (Figure 3; Text S1).

Seismic waveforms that are bandpass filtered between 0.004 and 8.0 Hz display an energy composition dominated by low-frequency energy. The *P* and *S* energies are dominant at frequencies of 0.004–0.03 Hz (Figure 6a, 6b). On the other hand, surface waves are dominant at frequencies of 0.004–0.08 Hz, and characteristic dispersion is observed for the surface waves. The permanent displacements and very-long-period waves are observed at frequencies of less than 0.004 Hz.

The energy pertaining to very-long-period seismic waves dissipates slowly with distance. The very-long-period energy generated by the megathrust earthquake travels throughout the Earth, producing displacements reaching a couple of centimeters around the antipole (Figure 1).

We analyze the ground motions by the September 12, 2016 M_L5.8 (M_W5.4) Gyeongju earthquake for comparison with those by the Tohoku-Oki earthquake. The seismic energy in the ground motions is hardly observed at frequencies less than 0.03 Hz (Figure 6c, 6d; Text S1). This may be because low-frequency energy is excited less from the Gyeongju earthquake. We separate the ground motions into two frequency bands of 0.03–0.08 Hz and > 0.08 Hz. The seismic energy of the Gyeongju earthquake is dominant at frequencies of > 0.08 Hz (mainly, 0.1–10 Hz; Hong, Lee, Kim, et al., 2017). Permanent displacements are rarely observed at regional stations. The ground motions are strongest in the surface waves.

7. Peak Ground Motions

The PGA and PGV are often used for the instrumental estimation of seismic intensity, which represents the level of seismic damage (Atkinson & Kaka, 2007; Atkinson & Sonley, 2000; Wald et al., 1999; Yaghmaei-Sabegh et al., 2011). Here, the PGA is generally analyzed for instrumental seismic-intensity measurement regardless the distance. On the other hand, the instrumental seismic-intensity measurement based on

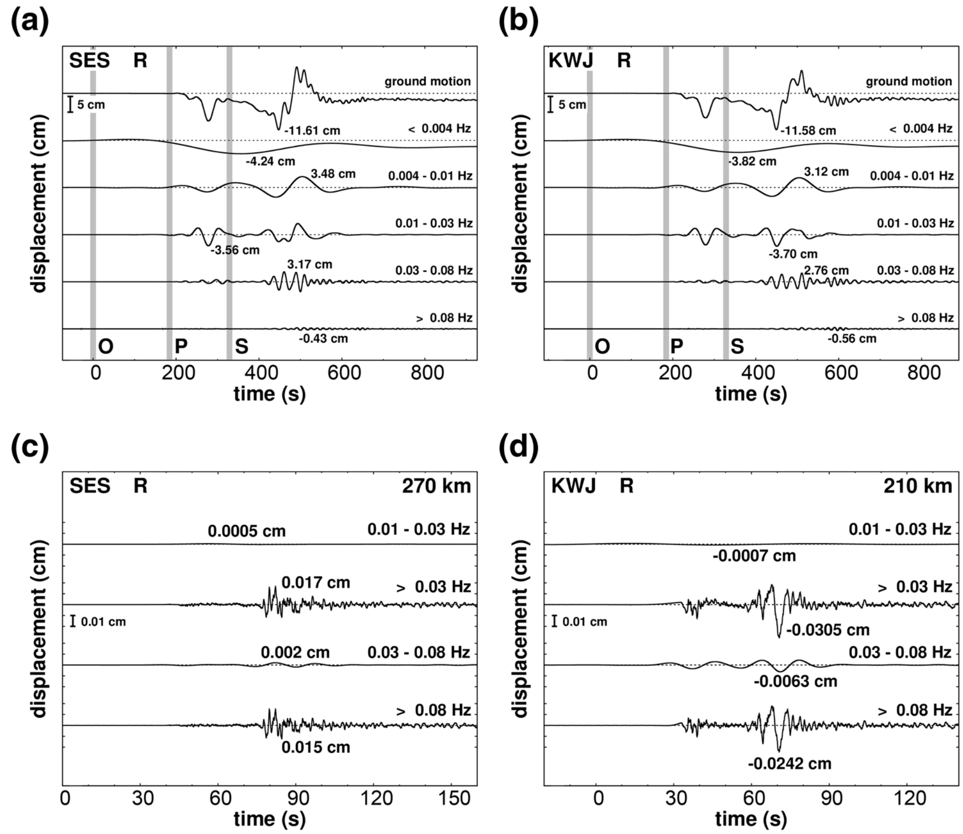

Figure 6. Radial displacement record sections by frequency band at stations (a) SES and (b) KWJ for the March 11, 2011 M_W9.0 Tohoku-Oki megathrust earthquake, and (c), (d) those for the September 12, 2016 M_L5.8 (M_W5.4) Gyeongju earthquake. The peak amplitudes are annotated. The ground motions by the Tohoku-Oki earthquake are dominant at frequencies of less than 0.08 Hz. The energy at frequencies of 0.03–0.08 Hz for the Tohoku-Oki earthquake is contained mostly within the surface waves. The origin time of the Tohoku-Oki earthquake (O) and the arrival times of *P* and *S* waves (P and S) are indicated. Seismic energy from the Gyeongju earthquake is dominant at frequencies greater than 0.08 Hz. The energy is rare at frequencies less than 0.03 Hz. The epicentral distances (210 and 270 km) and peak amplitudes are annotated.

PGV is often employed for local and near-regional earthquakes. The instrumental seismic intensities based on PGA and PGV are measured similar in local and near-regional regions (Atkinson & Kaka, 2007; Atkinson & Sonley, 2000; Wald et al., 1999; Yaghmaei-Sabegh et al., 2011).

A megathrust earthquake produces strong long-period ground motions. The influence of frequency contents of ground motions on seismic hazards was poorly understood. We examine the properties and potential seismic hazards of strong long-period motions from the Tohoku-Oki earthquake.

We prepare unclipped seismic records from accelerometers for the March 11, 2011 M_W9.0 Tohoku-Oki megathrust earthquake. The seismic records are band-pass filtered in 0.004–30 Hz where the energy is mostly composed of transient seismic waves. We measure the PGA, PGV, and PGD produced by the Tohoku-Oki earthquake. The horizontal and vertical PGAs corresponding to the megathrust earthquake range from 0.28 to 0.74 cm/s^2 and from 0.34 to 0.81 cm/s^2, respectively (Figure 7a; Text S1). The horizontal and vertical PGVs are in the ranges of 0.40–2.48 cm/s and 0.06–2.42 cm/s (Figure 7b; Text S1). The horizontal and vertical PGDs of the megathrust earthquake range from 3.26 to 19.93 cm and from 4.31 to 22.35 cm, respectively (Figure 7c; Text S1).

We further compare the peak ground motions induced by a megathrust earthquake in regional distance with those induced by a moderate-size earthquake in local distance. We find that the observed PGVs in the Korean Peninsula for the Tohoku-Oki earthquake are comparable to the PGVs generated by a M7

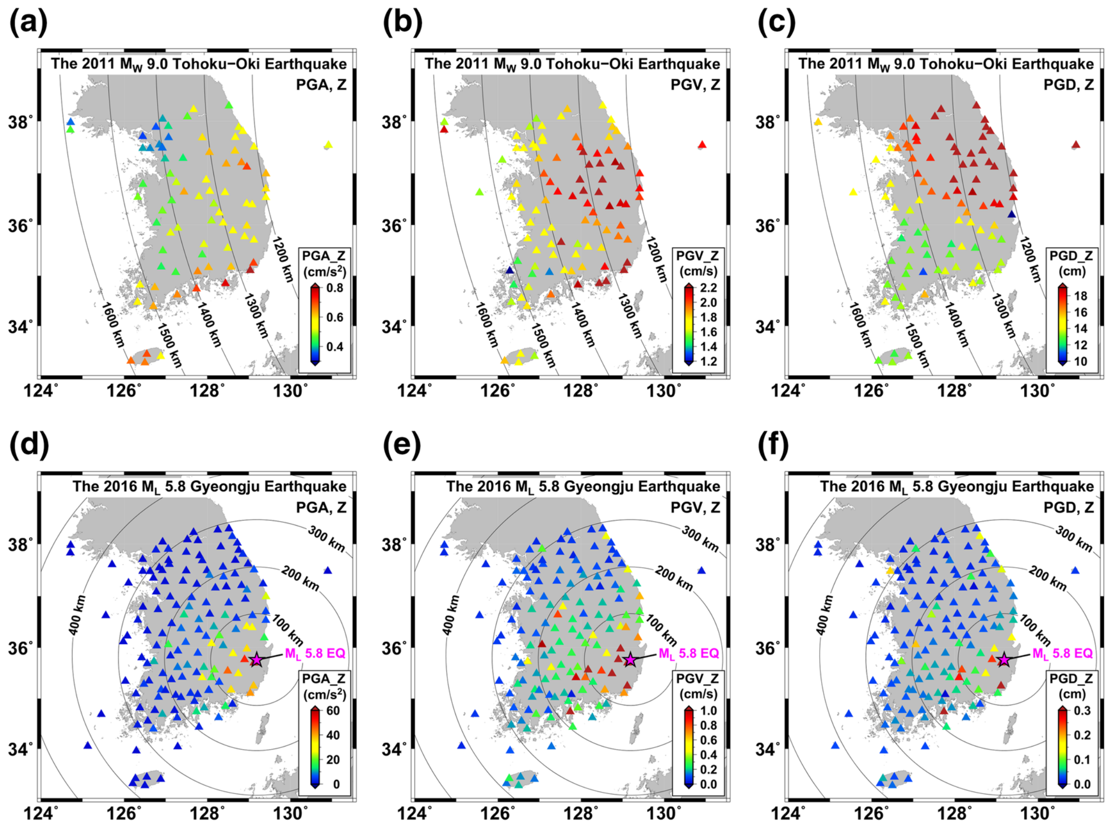

Figure 7. (a) Vertical peak ground accelerations (PGAs), (b) peak ground velocities (PGVs), and (c) peak ground displacements (PGDs) for the Tohoku-Oki earthquake, and (d, e, and f) those for the Gyeongju earthquake. The PGAs for the Gyeongju earthquake at local distances are much stronger than those for the Tohoku-Oki earthquake at far-regional distances. The PGVs for the Gyeongju earthquake at local distances are comparable to those for the Tohoku-Oki earthquake at far-regional distances. The PGDs for the Gyeongju earthquake at local distances are much weaker than those for the Tohoku-Oki earthquake at far-regional distances.

earthquake at local distances (Viens & Denolle, 2019; Yamada & Iwata, 2005). The level of ground motions for the observed PGVs is equivalent to seismic intensities of 4–5 on the Modified Mercalli Intensity (MMI) scale at local and regional distances (Atkinson & Kaka, 2007; Tselentis & Danciu, 2008; Wald et al., 1999). On the other hand, the level of the observed PGAs corresponds to seismic intensities ≤ MMI 1 according to the relationship between the PGA and seismic intensity in the Korean Peninsula (Park & Hong, 2017).

The levels of peak ground motions (PGA, PGV, and PGD) are dependent on the dominant frequency, event magnitude, and distance. We find characteristic differences in the peak ground motions between local moderate-size earthquake and regional megathrust earthquake. It was reported that the seismic damages (seismic intensity) may be dependent on PGV and PGA (Atkinson & Sonley, 2000; Dangkua & Cramer, 2011; Yaghmaei-Sabegh et al., 2011). However, despite comparable PGVs, seismic damages occur only in the regions with high PGAs. The observation suggests that PGA may be the most important factor for seismic damages. Also, the observation presents that the level of PGVs by a regional megathrust earthquake can be significant.

The discrepancy between PGA-based seismic intensities and PGV-based seismic intensities may be associated with discriminative frequency-dependent attenuation of seismic energy with distance. Strong attenuation of high frequency energy occurs in far-regional distance. The low PGA-based seismic intensities are consistent with no apparent seismic damages in the Korean Peninsula. The observation suggests that the PGV decays slowly with distance, producing large amplitudes in far-regional distances.

The peak ground motions present azimuth-dependent variations (Figure 8a, 8b). The PGDs on the tangential component are more amplified in the southern peninsula than in the central peninsula. On the other hand, the vertical PGDs in the central peninsula are larger than those in the southern peninsula (Figure 8c).

10.1029/2020JB020628

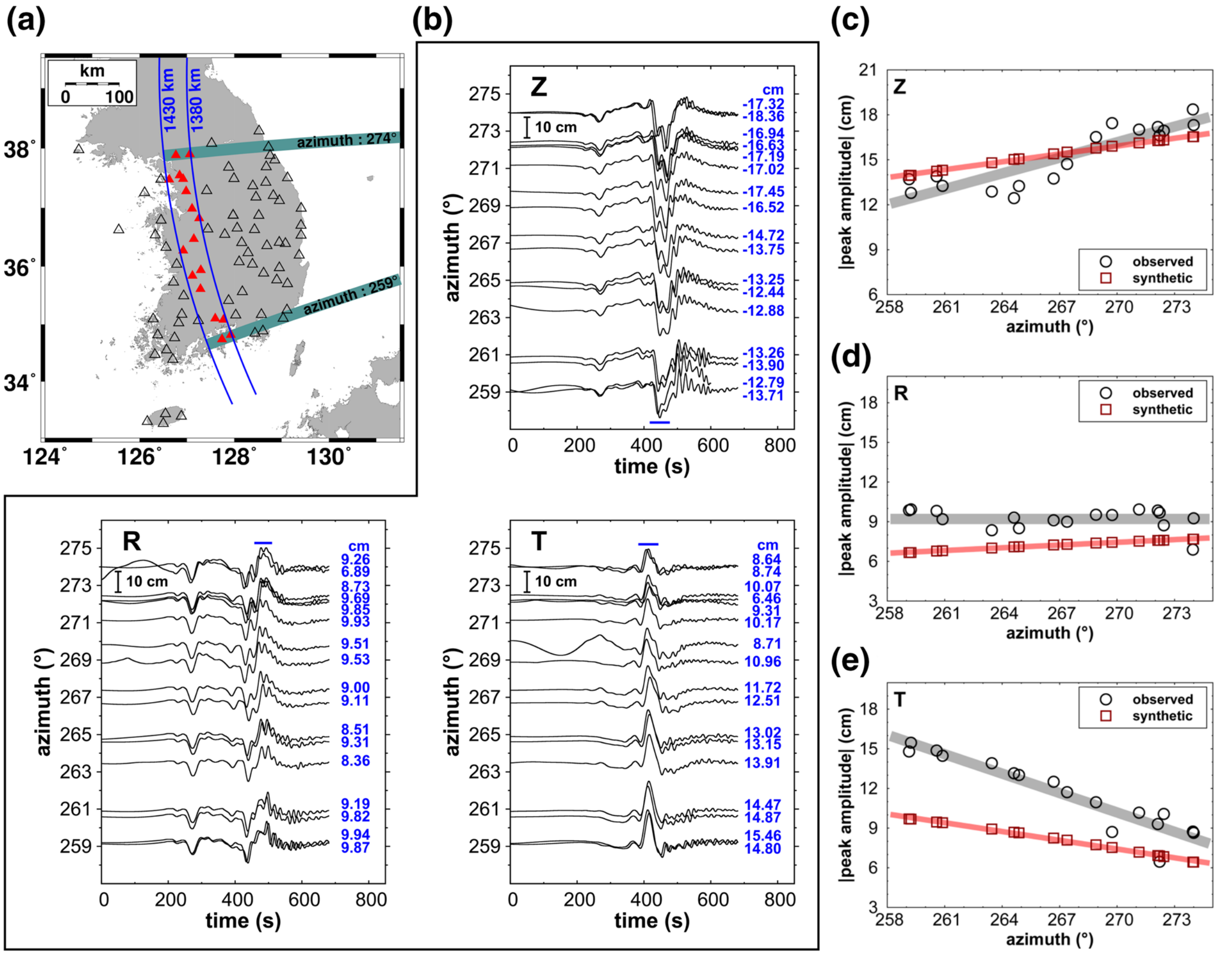

Figure 8. Azimuthal variations in the peak ground displacements for the Tohoku-Oki earthquake: (a) map of the stations, (b) ground motions in three components, and comparison of azimuthal PGD variations between field observations and synthetic waveforms: (c) vertical, (d) radial, and (e) tangential components. Stations analyzed (filled triangles on the map) are placed in distances between 1,380 and 1,430 km. Synthetic waveforms are presented in Figure 9. The PGDs of indicated phases (marked with bars) are annotated on the waveform records. The vertical PGD increases with azimuth, while the tangential PGD decreases with azimuth. The azimuthal-variation features in peak amplitudes of synthetic waveforms are consistent with the field observation. The amplitudes of synthetic waveforms are slightly lower than those of field observation due to point-source approximation. PGD, peak ground displacement.

These findings suggest that the peak tangential amplitude decreases with azimuth in the Korean Peninsula. In contrast, the peak vertical amplitude increases with azimuth (Figure 8c).

We calculate synthetic displacement waveforms in 0.004–0.1 Hz for a point source with the moment rate function and focal mechanism solution of the Tohoku-Oki earthquake (Wei et al., 2012; Yagi & Fukahata, 2011) using a frequency-wavenumber method (Saikia, 1994) based on a one-dimensional Earth model (Dziewonski & Anderson, 1981). We produce the synthetic displacement waveforms at a distance of 1,400 km for the azimuthal range (Figure 9).

We find that the amplitudes of synthetic waveforms are slightly smaller than those of field observation due to the implementation of a point source without consideration of fault rupture and directivity (Figure 8c). The PGDs are controlled by the characteristic radiation patterns of surface waves (Figure 9d). The radiation patterns of Rayleigh waves control the PGDs in the vertical and radial components. Also, the PGDs in the tangential component are dependent on the radiation patterns of Love waves. The azimuthal variations in peak amplitudes of synthetic waveforms are consistent with the field observation (Figure 8c).

We also find a characteristic amplitude variation along continental paths. The vertical PGD amplitudes decrease with distance due to natural geometrical spreading (Figures 10a and 10b). In contrast, the PGD amplitudes on the tangential component increase with distance in the continental region. Also, the PGDs

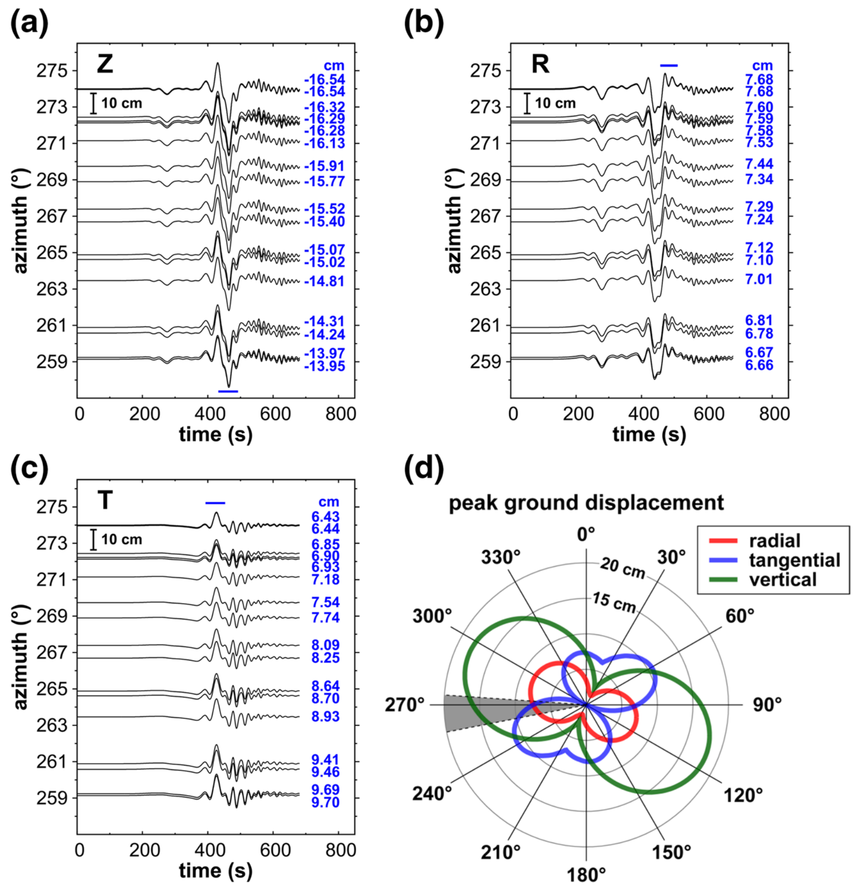

Figure 9. Azimuthal variations of synthetic waveforms and peak ground displacements for the Tohoku-Oki earthquake at stations in a distance of 1,400 km: synthetic waveforms in (a) vertical, (b) radial, and (c) tangential components, and (d) diagram for azimuth-dependent peak ground displacements of indicated phases. Synthetic waveforms are presented for stations at a distance of 1,400 km in the Korean Peninsula. The PGDs of indicated phases (marked with bars) are annotated on the waveform records. The azimuth range for the Korean Peninsula is marked in the PGD diagram. The vertical PGD increases with azimuth, while the tangential PGD decreases with azimuth. A point source with the moment rate function (Wei et al., 2012) is considered for the modeling of synthetic waveforms. PGD, peak ground displacement.

on the radial component mildly increase with distance in 1,250–1,500 km. The increasing amplitudes in tangential and radial components may be caused by the focusing and defocusing effect of wavefield due to the interference with crustal and upper mantle structures (Hong, 2014; Kennett, 1986; Kennett & Furumura, 2001). Also, the wavefield redevelopment after passage of complex media may play additional role in seismic-amplitude increase. It is noteworthy that the increasing amplitudes with distance are not associated with multi-phase arrivals such as *SS* and *S* caustics considering their traveltimes.

The continental crust in the Korean Peninsula changes abruptly to a transitional structure between continental crust and oceanic crust in the East Sea (Hong, 2010; Hong et al., 2008). Further, the crustal structure is laterally heterogeneous in the East Sea (Sea of Japan) due to continental rifting that occurred during the Oligocene to mid-Miocene (Chough et al., 2000). Crustally-guided waves and surface waves attenuate rapidly when they propagate through laterally heterogeneous crustal and upper mantle structures. The crustally guided waves and surface waves start to develop stably in the continental crust (Hong, 2014; Kennett, 1986; Kennett & Furumura, 2001).

The September 12, 2016 M_L5.8 (M_W5.4) Gyeongju earthquake is the largest earthquake since 1978 when the national seismic monitoring began (Hong, Lee, Kim, et al., 2017, 2018). The Gyeongju earthquake produced large seismic damages in local regions. In contrast, the Tohoku-Oki earthquake produced no seismic damages in the Korean Peninsula. We compare the peak ground motions by the Tohoku-Oki megathrust

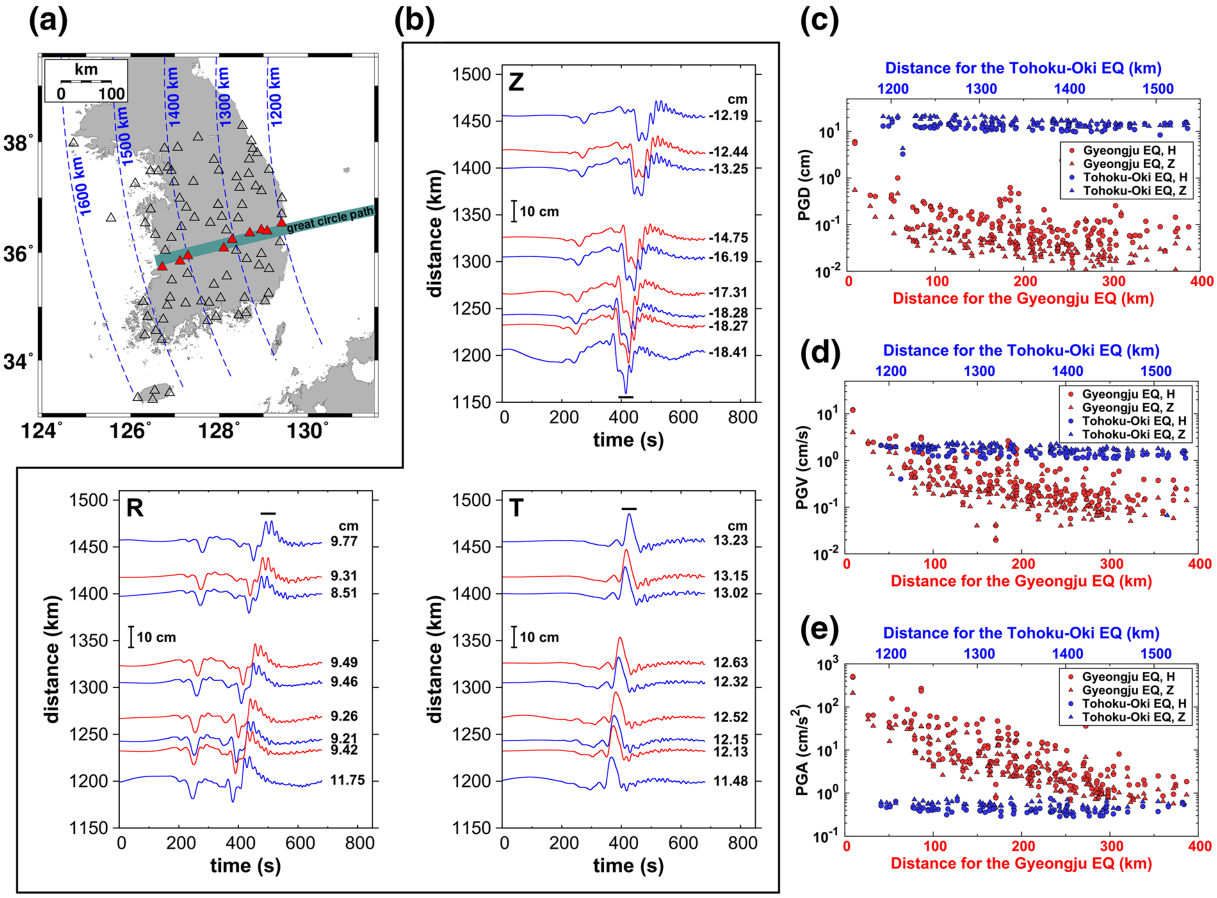

Figure 10. Ground motion variation with distance along a common great-circle path: (a) map of the stations, and (b) ground motions in three-components. Blue and red lines are used for every two records to distinguish the waveforms. The vertical PGD decreases with distance due to geometrical spreading, while the tangential PGD increases with distance. Comparison of peak ground motions between the Tohoku-Oki earthquake and the Gyeongju earthquake: (c) PGD, (d) PGV, and (e) PGA. Stations analyzed are marked on map (filled triangles). The PGDs and PGVs for the Tohoku-Oki earthquake are larger than those for the Gyeongju earthquake. The PGAs for the Tohoku-Oki earthquake are smaller than those for the Gyeongju earthquake. PGA, peak ground acceleration; PGD, peak ground displacement; PGV, peak ground velocities.

earthquake with those by the Gyeongju earthquake to identify the differences in the properties of ground motions.

The seismic data are filtered between 0.03 and 30 Hz considering the frequency contents of seismic energy. Most seismic energy is in frequencies greater than 0.03 Hz (Figures 6c and 6d). The horizontal and vertical PGAs of the Gyeongju earthquake were 0.38–509.64 cm/s^2 and 0.33–210.12 cm/s^2, respectively (Figure 7d; Text S1). The horizontal and vertical PGVs were 0.01–12.17 cm/s and 0.02–3.98 cm/s (Figure 7e; Text S1). The horizontal and vertical PGDs were 0.003–6.05 cm and 0.002–0.55 cm (Figure 7f; Text S1). The instrumental seismic intensities for the Gyeongju earthquake reached MMI 9 around the epicenter (Hong, Lee, Kim, et al., 2017).

The PGVs can be converted to peak dynamic strains and peak dynamic stress changes induced in the media. We consider two representative depths of 10 and 60 km for the crust and upper mantle. We set the shear-wave velocities (V_s) and shear moduli (μ) to be 3.58 km/s and 34.95 GPa for a depth of 10 km, 4.48 km/s and 67.04 GPa for a depth of 60 km considering the medium properties in the Korean Peninsula (Chang & Baag, 2006; Houng et al., 2016; Jo & Hong, 2013). The peak dynamic strains are 2.79×10^{-8} to 3.40×10^{-5} for a depth of 10 km, and 2.79×10^{-8} to 2.72×10^{-5} for a depth of 60 km. The peak dynamic stress changes reach 1.18 MPa for a depth of 10 km, and 1.82 MPa for a depth of 60 km. The dynamic stress changes for a depth of 10 km are greater than the typical stress changes required for dynamic earthquake triggering in the crust (Hill & Prejean, 2007). The observation is consistent with the rapid increase of dynamically-triggered earthquakes in the Korean Peninsula (Houng et al., 2016).

The PGDs of the Tohoku-Oki earthquake at far-regional distances (∼1,200–1,500 km) are ∼20–500 times larger than those of the Gyeongju earthquake at all distances (Figure 10c). The PGVs around the eastern coast of the Korean Peninsula for the Tohoku-Oki earthquake correspond to PGVs at tens of kilometers for the Gyeongju earthquake (Figures 7 and 10d). The PGVs of the Tohoku-Oki earthquake mildly decrease with distance at far-regional distances (∼1,200–1,500 km). The levels of PGVs of the Tohoku-Oki earthquake at distances of ∼1,200 km are comparable to those of the Gyeongju earthquake at distances of ∼50 km (Figure 10d). On the other hand, the PGAs of the Gyeongju earthquake at distances of ≤ 50 km are ∼100–1,000 times larger than those of the Tohoku-Oki earthquake at far-regional distances (∼1,200–1,500 km; Figure 10e).

The observation presents that the PGDs and PGVs for a megathrust earthquake at far-regional distances can be larger than those for a moderate-size earthquake at local distances. In contrast, the PGAs for a megathrust earthquake at far-regional distances are much smaller than those for a moderate-size earthquake at local distances. It is known that the Gyeongju earthquake caused considerable seismic damage at local distances. On the other hand, the Tohoku-Oki megathrust earthquake caused little seismic damage in the Korean Peninsula. The levels of observed seismic damages are reasonably estimated with PGAs.

The observation suggests that the seismic damages may be more dependent on PGA than PGV. It is noteworthy that the seismic intensities (seismic damages) in the Korean Peninsula could be well determined based on PGAs (Hong et al., 2019; Park & Hong, 2017). However, the long-period ground motions produced by the Tohoku-Oki earthquake may affect high-rize buildings and structures of which natural frequencies are low. The high-rise buildings and structures may be dynamically distorted in long duration by the long-period ground motions.

The large PGDs and PGVs for the Tohoku-Oki earthquake at far-regional distances are caused by large long-period energy that decays slowly with distance. The large long-period energy displacements may cause stress loading and release in the subsurface media. It was reported that the strong long-period ground motions excited by the Tohoku-Oki earthquake incurred large dynamic stress changes in the crust of the Korea Peninsula, triggering a large number of small events (Houng et al., 2016). Also, the permanent displacements cause static stress changes in the media. This feature agrees with the apparent increase in seismicity in the crust of the Korean Peninsula after the megathrust earthquake (Hong et al., 2015, 2018; Hong, Park, Lee, Chung, et al., 2020; Hong, Park, Lee, & Kim, 2020). The persistent long-period energy produced by a megathrust earthquake may load displacements and stress on high-rise buildings that have low natural frequencies.

8. Influence of Long-Period Waves on Subsurface Media

Long-period dynamic ground motions may cause moderate perturbations in the subsurface media, which subsequently cause changes in the stress field and seismicity (Johnson & Jia, 2005). We observe large long-period ground motions at frequencies of less than 0.03 Hz, which may affect the upper mantle. The mantle is composed of olivine with various grain sizes that may exhibit a frequency-dependent response to dynamic motions (Solomatov & Reese, 2008). In particular, slow dynamics are effective on most Earth materials (TenCate, 2011). Seismic velocities may recover linearly with logarithmic time (Peng & Ben-Zion, 2006).

We examine whether the subsurface media were perturbed by the long-period ground motions. We first determine the traveltime changes of Rayleigh waves from closely-located events before and after the March 11, 2011 Tohoku-Oki megathrust earthquake (Figure 11). We choose three events with similar focal mechanisms, magnitudes (M_W5.3–6.1), and focal depths (41–45 km) that occurred near the Tohoku-Oki earthquake. The doublet events are located ∼139–140 km in SW from the Tohoku-Oki earthquake.

We collect seismic records from stations ULLB and BAR (Figure 11). The seismic waveforms are bandpass filtered between 0.01 and 0.03 Hz. We compare the seismic waveforms before and after the Tohoku-Oki earthquake. We find no apparent traveltime changes in seismic phases including P and Rayleigh waves at both stations (ULLB and BAR). The misfit in amplitudes before and after the Rayleigh waves in station

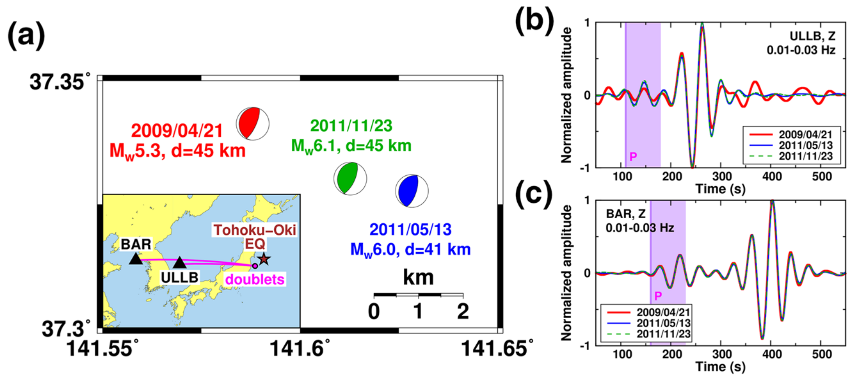

Figure 11. Seismic waveforms of three closed-located events before and after the Tohoku-Oki earthquake: (a) map of events and stations, and comparison of vertical seismic waveforms in frequencies of 0.01–0.03 Hz at stations (b) ULLB and (c) BAR. The events share similar focal mechanism solutions. The magnitudes and focal depths are annotated. The interevent distances are 2.5–5.9 km. There are no apparent differences in surface-wave traveltimes at frequencies of 0.01–0.03 Hz between the two stations.

ULLB may be caused by site ambient noises and event magnitude difference. The distances between the Tohoku-Oki earthquake and stations are ~1,050 and ~1,587 km. Also, the distances between the doublet events and stations are ~944 km and ~1,487 km. The great-circle paths between doublet events and stations are close to those between the Tohoku-Oki earthquake and stations (Figure 11).

We now measure the traveltime changes of Rayleigh waves using ambient noise cross-correlation analysis. We choose a station pair (broadband velocity stations ULLB and BAR) placed close to the orientation of a great-circle arc with the megathrust earthquake (Figure 12). The interstation path is placed across the central Korean Peninsula. He interstation distance between ULLB and BAR is 554 km. We collect continuous vertical seismic records of this station pair from June 2010 to December 2012.

We retrieve the Green's functions at frequencies of 0.01–0.03 Hz from ambient noise cross-correlation analysis (Figure 12). We calculate the vertical noise cross-correlation functions based on the noise records in 1st–3rd days, 4th–8th days, 9th–23rd days, 24th–63rd days, 64th–103rd days, 104th–183rd days, 184th–263rd days, 364th–463rd days, 464th–563rd days, and 564th–660th days after the Tohoku-Oki earthquake. Here,

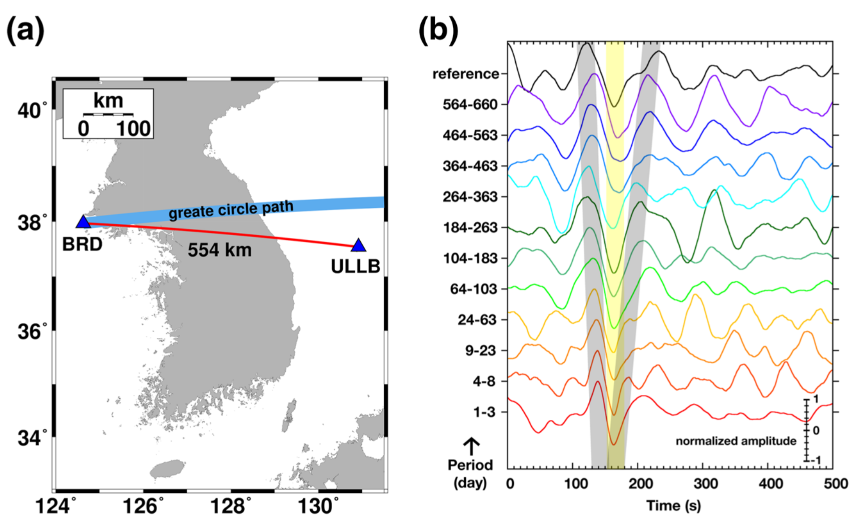

Figure 12. Ambient noise cross-correlation functions for a station pair (ULLB and BAR): (a) map of the stations and interstation path and (b) variations in the noise cross-correlation functions with time. The time period is annotated in days. Different line colors are used to distinguish the waveforms. Waveform shortening is observed right after the megathrust earthquake. The waveforms revert back to the reference waveforms with time. The zero phase in the wavelet is shaded.

we use longer time periods with lapse time after the Tohoku-Oki earthquake considering the general medium-property recovery rate with time (Hong, Lee, Chi, et al., 2017). We also calculate the reference noise cross-correlation function based on the noise records over 213 days from June 1, 2010 to December 31, 2010.

We examine the frequency contents in the noise cross-correlation functions (Figure 12). We observe apparent frequency changes in the noise cross-correlation functions with time (Figure 12b). The noise cross-correlation functions after the Tohoku-Oki earthquake present higher frequency contents relative to the reference noise cross-correlation function before the Tohoku-Oki earthquake. The frequency contents of the noise cross-correlation functions were shifted higher immediately after the megathrust earthquake. The apparent frequency-content change is gradually recovered with time. The apparent frequency content converges to the usual content for two years after the megathrust earthquake.

We, however, observe that the zero-phase traveltimes of the Rayleigh waves are nearly constant before and after the Tohoku-Oki earthquake (Figure 12b). The observation suggests that the phase velocity is invariant. Also, the long-period dynamic deformation rarely changed the long-period Green's function. The invariant phase velocities of long-period wave from noise cross-correlation functions are consistent with those observed from the doublet-event analysis.

The apparent frequency content changes after the Tohoku-Oki earthquake may be due to high postseismicity in the source region (Tajima et al., 2013). Aftershocks produce seismic energy, changing the apparent distribution of seismic sources that contribute to the ambient noise field. Successive inflows of seismic energy cause apparent change in the spectral content (Bensen et al., 2007). The increase in seismic-energy inflow mimics a situation in which the noise sources proceed to the receiver. This situation causes apparent frequency increase in observed waveforms.

The number of aftershocks in the source region decreases gradually with time. The decreasing aftershocks causes apparent weakening of seismic-energy inflow in the ambient seismic-noise field. The temporal seismic energy decrease composes a situation in which the noise sources recede from the receiver. The situation causes apparent frequency decrease in observed waveforms. Thus, the postseismicity occurrence after the Tohoku-Oki earthquake and its temporal decay cause apparent frequency content change (Doppler shift). The observation suggests that the postseismicity effectively contributes to compose the long-period ambient seismic-noise field in far-regional distances. However, long-period displacements produced by a megathrust earthquake appear to perturb rarely the medium properties and stress field in the mantle.

9. Discussion and Conclusions

The excitation of elastogravity waves by a megathrust earthquake was identified in recent studies (Montagner et al., 2016; Vallée et al., 2017). However, the nature and influence of the elastogravity waves remain poorly understood. In particular, the ground motions induced by a megathrust earthquake are a mixture of elastogravity waves, seismic waves and permanent displacements. The inherent light-speed propagation of elastogravity waves and low attenuation of long-period waves naturally produce long wavetrains. The hazard potentials of the combined long-period ground motions are still unknown.

We investigated the dynamic ground motions in the Korean Peninsula that were excited by the 2011 M_W9.0 Tohoku-Oki megathrust earthquake at a far-regional distance. The dynamic ground motions in the full frequency range were retrieved from unclipped broadband velocity seismograms of two stations using a time-domain instrument response correction method. The dynamic ground motions in the Korean Peninsula for the Tohoku-Oki earthquake were dominated by low-frequency energy (less than 0.1 Hz). The retrieved permanent displacements are consistent with geodetic observations (Baek et al., 2012; Hong et al., 2015; Shao et al., 2016; Zhao et al., 2012). The coseismic permanent displacements were produced ~600 s after the P arrival times.

Transient seismic waves produced large ground displacements during their passage across the Korean Peninsula. The P and S energies were dominant at frequencies of 0.004–0.03 Hz. Very-long-period (<0.004 Hz) wave trains are a mixture of transient seismic waves, elastogravity waves and permanent displacements (static deformation). Transient seismic waves after the P arrival times displayed radially polarized retrograde particle motions for ~600 s.

Elastogravity waves developed promptly at the origin time of the Tohoku-Oki earthquake. The elastogravity waves could be clearly distinguished before the *P* arrivals at frequencies of < 0.004 Hz. These elastogravity waves were dominant along the great-circle paths to the Tohoku-Oki earthquake and presented prograde particle motions. The elastogravity waves were mixed with very-long-period seismic waves after the *P* arrival times. The strength of elastogravity waves may be dependent on the magnitude of mass dislocation. The characteristic waveform features of elastogravity waves may enable us to detect small to moderate-size mass-dislocation events such as earthquakes, landslides, and bolide impacts.

We analyzed the peak ground motions at frequencies of 0.004–30 Hz using the seismic records from 101 accelerometers that are distributed homogeneously over the Korean Peninsula. The peak ground motions presented characteristic differences between far-regional megathrust earthquake and local moderate-size earthquake. The PGAs for the Tohoku-Oki earthquake at far-regional distances were lower than those for the Gyeongju earthquake at local and near-regional distances. The PGVs for the megathrust earthquake were comparable to those for the moderate-size earthquake. On the other hand, the PGDs for the megathrust earthquake were much larger than those for the moderate-size earthquake.

The PGDs generated by the Tohoku-Oki earthquake exceeded 20 cm in the eastern Korea Peninsula and ±15 cm in the western peninsula. These large ground displacements were not perceived by people due to slow ground motions with periods of ∼200 s. The PGVs for the Tohoku-Oki earthquake were considerably large, producing high dynamic stress changes of ∼1.1 MPa in the curst and ∼ 1.8 MPa in the lithosphere. It is noteworthy that the Gyeongju earthquake caused dynamic stress changes of < 0.1 MPa in the suburb of the source region (Hong, Lee, Kim, et al., 2017).

Megathrust earthquakes may produce large ground motions from local to teleseismic distances. The PGDs reach ∼1 cm in the antipodal regions. The displacement ground motions produced by the Tohoku-Oki earthquake are dominant at frequencies ≤ 0.03 Hz in the Korean Peninsula. Current skyscrapers in the world generally have natural frequencies of ≥0.05 Hz. Higher skyscrapers may be more affected by the megathrust earthquakes. However, the dynamic ground motions by the megathrust earthquakes are dominantly composed of low frequency energy. Thus, PGD and PGV may be major factors to be considered for earthquake-resistant design of skyscrapers for megathrust earthquakes.

The dynamic ground motions displayed characteristic azimuth- and distance-dependent features. The peak ground motions presented azimuthal variations following the source radiation pattern and moment-rate function. The tangential PGD increased with distance due to the development of crustally guided phases and surface waves along continental paths. On the other hand, the vertical PGD attenuated with distance due to geometrical spreading. The dynamic motions were dominated by low frequency energy. Medium properties were scarcely affected by the strong low-frequency motions.

The strong long-period ground motions induced by megathrust earthquakes suggest possible large long-duration distortions that may be particularly effective on large structures and buildings. The large long-period distortions appear to occur in regional to teleseismic distances. Modern buildings and structures become bigger. Large structures may be affected by the long-period displacements.

Data Availability Statement

The data and results of this study are available in the following repository (https://doi.org/10.5061/dryad.5tb2rbp39). The seismic records were collected from the Korean Meteorological Administration (KMA) and Korea Institute of Geoscience and Mineral Resources (KIGAM).

Acknowledgments
The authors thank Dr Rachel Abercrombie (editor), associate editor, Dr Iris van Zelst (reviewer), and two anonymous reviewers for fruitful review comments to improve the presentation of the manuscript. This work was supported by the Korea Meteorological Administration Research and Development Program under grant KMI2018-02910. Additionally, this research was partly supported by the Basic Science Research Program of National Research Foundation of Korea (NRF-2017R1A6A1A07015374 and NRF-2018R1D1A1A09083446).

References

Anderson, J. F., & Lees, J. M. (2014). Instrument corrections by time-domain deconvolution. *Seismological Research Letters*, *85*(1), 197–201.

Atkinson, G., & Kaka, S. (2007). Relationship between felt intensity and instrumental ground motion in the central United States and California. *Bulletin of the Seismological Society of America*, *97*(2), 497–510.

Atkinson, G., & Sonley, E. (2000). Empirical relationships between modified Mercalli intensity and response spectra. *Bulletin of the Seismological Society of America*, *90*, 537–544.

Baek, J., Shin, Y. H., Na, S. H., Shestakov, N. V., Park, P. H., & Cho, S. (2012). Coseismic and postseismic crustal deformations of the Korean Peninsula caused by the 2011 Mw 9.0 Tohoku earthquake, Japan, from global positioning system data. *Terra Nova*, *24*(4), 295–300.

Bensen, G. D., Ritzwoller, M. H., Barmin, M. P., Levshin, A. L., Lin, F., Moschetti, M. P., et al. (2007). Processing seismic ambient noise data to obtain reliable broad-band surface wave dispersion measurements. *Geophysical Journal International*, *169*, 1239–1260.

Birch, F. (1960). The velocity of compressional waves in rocks to 10 kilobars, part 1. *Journal of Geophysical Reseearch*, *65*, 1083–1102.

Boore, D. M. (2001). Effect of baseline corrections on displacements and response spectra for several recordings of the 1999 Chi-Chi, Taiwan, earthquake. *Bulletin of the Seismological Society of America*, *91*(5), 1199–1211.

Campillo, M., & Paul, A. (2003). Long-range correlations in the diffuse seismic coda. *Science*, *299*, 547–549.

Caskey, S. J., & Wesnousky, S. G. (1997). Static stress changes and earthquake triggering during the 1954 Fairview Peak and Dixie Valley earthquakes, central Nevada. *Bulletin of the Seismological Society of America*, *87*(3), 521–527.

Chang, S.-J., & Baag, C.-E. (2006). Crustal structure in southern Korea from joint analysis of regional broadband waveforms and travel times. *Bulletin of the Seismological Society of America*, *96*, 856–870.

Chough, S. K., Kwon, S.-T., Ree, J.-H., & Choi, D. K. (2000). Tectonic and sedimentary evolution of the Korean peninsula: a review and new view. *Earth-Science Reviews*, *52*, 175–235.

Dangkua, D. T., & Cramer, C. H. (2011). Felt intensity versus instrumental ground motion: A difference between California and eastern North America? *Bulletin of the Seismological Society of America*, *101*(4), 1847–1858.

Dziewonski, A. M., & Anderson, D. L. (1981). Preliminary reference Earth model. *Physics of the Earth and Planetary Interiors*, *25*(4), 297–356.

Ellis, B. R. (1980). An assessment of the accuracy of predicting the fundamental natural frequencies of buildings and the implications concerning the dynamic analysis of structures. *Proceedings of the Institution of Civil Engineers*, *2*(69), 763–776.

Gautam, P. K., Sathyaseelan, R., Pappachen, J. P., Kumar, N., Biswas, A., Philip, G., et al. (2019). GPS measured static and kinematic offsets at near and far field of the 2011 Mw 9.0 Tohoku-Oki earthquake. *Geodesy and Geodynamics*, *10*(3), 213–227.

Gomberg, J., Reasenberg, P. A., Bodin, P. L., & Harris, R. A. (2001). Earthquake triggering by seismic waves following the Landers and Hector Mine earthquakes. *Nature*, *411*(6836), 462–466.

Guo, A., Wang, Y., Li, Z., Ni, S., Wu, W., Liu, G., et al. (2013). Observation of core phase ScS from the Mw9.0 Tohoku-Oki earthquake with high-rate GPS. *Seismological Research Letters*, *84*(4), 594–599.

Haney, M. M., Power, J., West, M., & Michaels, P. (2012). Causal instrument corrections for short-period and broadband seismometers. *Seismological Research Letters*, *83*(5), 834–845.

Harms, J., Ampuero, J.-P., Barsuglia, M., Chassande-Mottin, E., Montagner, J.-P., Somala, S. N., & Whiting, B. F. (2015). Transient gravity perturbations induced by earthquake rupture. *Geophysical Journal International*, *201*, 1416–1425.

Heaton, T., Hall, J., Wald, D., & Halling, M. (1995). Response of high-rise and base-isolated buildings to a hypothetical M 7.0 blind thrust earthquake. *Science*, *267*, 206–211.

Hill, D. P., & Prejean, S. G. (2007). Dynamic triggering. In H. Kanamori (Ed.), *Earthquake seismology, treatise on geophysics* (Vol. 4, pp. 257–291). Amsterdam: Elsevier.

Hill, D. P., Reasenberg, P. A., Michael, A., Arabaz, W. J., Beroza, G., Brumbaugh, D., et al. (1993). Seismicity remotely triggered by the magnitude 7.3 Landers, California, earthquake. *Science*, *260*(5114), 1617–1623.

Hong, T.-K. (2010). Lg attenuation in a region with both continental and oceanic environments. *Bulletin of the Seismological Society of America*, *100*(2), 851–858.

Hong, T.-K. (2014). Influence of continental margin on regional seismic wavefield. *Tectonophysics*, *627*, 141–158.

Hong, T.-K., Baag, C.-E., Choi, H., & Sheen, D.-H. (2008). Regional seismic observations of the 9 October 2006 underground nuclear explosion in North Korea and the influence of crustal structure on regional phases. *Journal of Geophysical Research*, *113*, B03305. https://doi.org/10.1029/2007JB004950

Hong, T.-K., Lee, J., Chi, D., & Park, S. (2017). Seismic velocity changes in the backarc continental crust after the 2011 Mw 9.0 Tohoku-Oki megathrust earthquake. *Geophysical Research Letters*, *44*, 10997–11003. https://doi.org/10.1002/2017GL075447

Hong, T.-K., Lee, J., & Houng, S. E. (2015). Long-term evolution of intraplate seismicity in stress shadows after a megathrust. *Physics of the Earth and Planetary Interiors*, *245*, 59–70.

Hong, T.-K., Lee, J., Kim, W., Hahm, I. K., Woo, N. C., & Park, S. (2017). The 12 September 2016 M_L5.8 midcrustal earthquake in the Korean Peninsula and its seismic implications. *Geophysical Research Letters*, *44*(7), 3131–3138. https://doi.org/10.1002/2017GL072899

Hong, T.-K., Lee, J., Park, S., & Kim, W. (2018). Time-advanced occurrence of moderate-size earthquakes in a stable intraplate region after a megathrust earthquake and their seismic properties. *Scientific Reports*, *8*, 13331. https://doi.org/10.1038/s41598-018-31600-5

Hong, T.-K., Lee, J., Park, S., Yoon, H. H., Kim, W., & Shin, J. S. (2019). Seismic detection of strong ground motions by Mw5.6 North Korean nuclear explosion. *Scientific Reports*, *9*, 5124. https://doi.org/10.1038/s41598-019-41627-x

Hong, T.-K., Park, S., Lee, J., Chung, D., & Kim, W. (2020). One-off deep crustal earthquake swarm in a stable intracontinental region of the southwestern Korean Peninsula. *Physics of the Earth and Planetary Interiors*, *308*, 106582. https://doi.org/10.1016/j.pepi.2020.106582.

Hong, T.-K., Park, S., Lee, J., & Kim, W. (2020). Spatiotemporal seismicity evolution and seismic hazard potentials in the western East Sea (Sea of Japan). *Pure and Applied Geophysics*, *177*(8), 3761–3774.

Houng, S. E., Lee, J., & Hong, T. K. (2016). Dynamic seismic response of a stable intraplate region to a megathrust earthquake. *Tectonophysics*, *689*, 67–78.

Iwan, W. D., Moser, M. A., & Peng, C. Y. (1985). Some observations on strong-motion earthquake measurement using a digital accelerograph. *Bulletin of the Seismological Society of America*, *75*(5), 1225–1246.

Johnson, P. A., & Jia, X. (2005). Nonlinear dynamics, granular media and dynamic earthquake triggering. *Nature*, *437*(7060), 871–874.

Jo, E., & Hong, T.-K. (2013). Vp/Vs ratios in the upper crust of the southern Korean Peninsula and their correlations with seismic and geophysical properties. *Journal of Asian Earth Sciences*, *66*, 204–214.

Kanamori, H. (1979). A semi-empirical approach to prediction of long-period ground motions from great earthquakes. *Bulletin of the Seismological Society of America*, *69*, 1645–1670.

Kanamori, H., & Rivera, L. (2008). Source inversion of W phase: Speeding up seismic tsunami warning. *Geophysical Journal International*, *175*(1), 222–238.

Kennett, B. L. N. (1986). Lg waves and structural boundaries. *Bulletin of the Seismological Society of America*, *76*, 1133–1141.

Kennett, B. L. N., & Furumura, T. (2001). Regional phases in continental and oceanic environments. *Geophysical Journal International*, *146*(2), 562–568.

Kim, I., & Hong, T.-K. (2018). Azimuthal seismic anisotropy in the upper crust of the Japanese islands induced by the 2011 Tohoku-Oki megathrust earthquake. *Geophysical Research Letters*, *45*, 12793–12803. https://doi.org/10.1029/2018GL0807

Kim, D., Park, K. D., Ha, J., Sohn, D. H., & Won, J. (2016). Geodetic analysis of post-seismic crustal deformations occurring in South Korea due to the Tohoku-Oki earthquake. *KSCE Journal of Civil Engineering*, *20*, 2885–2892.

Koketsu, K., & Miyake, H. (2008). A seismological overview of long-period ground motion. *Journal of Seismology*, *12*, 133–143.
Lay, T., Ammon, C. J., Kanamori, H., Xue, L., & Kim, M. J. (2011). Possible large near-trench slip during the 2011 Mw9.0 off the Pacific coast of Tohoku Earthquake. *Earth Planets and Space*, *63*, 687–692.
Lee, W. H., Jennings, P., Kisslinger, C., & Kanamori, H. (Eds.), (2002). *International handbook of earthquake and engineering seismology*. Elsevier.
Matsuo, K., & Heki, K. (2011). Coseismic gravity changes of the 2011 Tohoku. Oki earthquake from satellite gravimetry. *Geophysical Research Letters*, *38*, L00G12. https://doi.org/10.1029/2011GL049018
Montagner, J.-P., Juhel, K., Barsuglia, M., Ampuero, J. P., Chassande-Mottin, E., Harms, J., et al. (2016). Prompt gravity signal induced by the 2011 Tohoku-Oki earthquake. *Nature Communications*, *7*, 13349. https://doi.org/10.1038/ncomms13349
Nakahara, H. (2015). Auto correlation analysis of coda waves from local earthquakes for detecting temporal changes in shallow subsurface structures: the 2011 Tohoku-Oki, Japan earthquake. *Pure and Applied Geophysics*, *172*(2), 213–224.
Nakata, N., & Snieder, R. (2011). Near-surface weakening in Japan after the 2011 Tohoku-Oki earthquake. *Geophysical Research Letters*, *38*, L17302. https://doi.org/10.1029/2011GL048800
Nur, A., & Simmons, G. (1969). The effect of saturation on velocity in low porosity rocks. *Earth and Planetary Science Letters*, *7*, 183–193.
Park, S., & Hong, T.-K. (2017). Regional seismic intensity anomalies in the Korean Peninsula and its implications for seismic-hazard potentials. *Pure and Applied Geophysics*, *174*(7), 2561–2579.
Parsons, T., Yeats, R. S., Yagi, Y., & Hussain, A. (2006). Static stress change from the 8 October, 2005 M=7.6 Kashmir earthquake. *Geophysical Research Letters*, *33*, L06304. https://doi.org/10.1029/2005GL025429
Pei, S., Niu, F., Ben-Zion, Y., Sun, Q., Liu, Y., Xue, X., et al. (2019). Seismic velocity reduction and accelerated recovery due to earthquakes on the Longmenshan fault. *Nature Geoscience*, *12*, 387–392.
Peng, Z., & Ben-Zion, Y. (2006). Temporal changes of shallow seismic velocity around the karadere-Duüzce branch of the North Anatolian fault and strong ground. *Pure and Applied Geophysics*, *163*, 567–600.
Pino, N. A., & Di Luccio, F. (2005). Seismic recording of small zero frequency displacement from moderate events. *Geophysical Research Letters*, *32*, L12304. https://doi.org/10.1029/2005GL022780
Psimoulis, P. A., Houlié, N., Habboub, M., Michel, C., & Rothacher, M. (2018). Detection of ground motions using high-rate GPS time-series. *Geophysical Journal International*, *214*(2), 1237–1251.
Psimoulis, P. A., Houlié, N., Michel, C., Meindl, M., & Rothacher, M. (2014). Long-period surface motion of the multipatch Mw9.0 Tohoku-Oki earthquake. *Geophysical Journal International*, *199*(2), 968–980.
Reasenberg, P. A., & Simpson, R. W. (1992). Response of regional seismicity to the static stress change produced by the Loma Prieta earthquake. *Science*, *255*(5052), 1687–1690.
Rossmann, J. S., Dym, C. L., & Bassman, L. (2015). *Introduction to engineering mechanics: A continuum approach* (2nd ed.). Boca Raton, FL: Taylor & Francis, CRC Press.
Saikia, C. K. (1994). Modified frequency-wavenumber algorithm for regional seismograms using Filon's quadrature: Modeling of Lg waves in eastern North America. *Geophysical Journal International*, *118*, 142–158.
Scherbaum, F. (2007). *Of Poles and zeros: Fundamentals of digital seismology* (revised 2nd ed.). Dordrecht: Springer.
Shao, Z., Zhan, W., Zhang, L., & Xu, J. (2016). Analysis of the far-field co-seismic and post-seismic responses caused by the 2011 Mw9.0 Tohoku-Oki Earthquake. *Pure and Applied Geophysics*, *173*(2), 411–424.
Shapiro, N. M., Campillo, M., Stehly, L., & Ritzwoller, M. H. (2005). High-resolution surface-wave tomography from ambient seismic noise. *Science*, *307*, 1615–1618.
Shestakov, N. V., Takahashi, H., Ohzono, M., Prytkov, A. S., Bykov, V. G., Gerasimenko, M. D., et al. (2012). Analysis of the far-field crustal displacements caused by the 2011 Great Tohoku earthquake inferred from continuous GPS observations. *Tectonophysics*, *524*, 76–86.
Solomatov, V. S., & Reese, C. C. (2008). Grain size variations in the Earth's mantle and the evolution of primordial chemical heterogeneities. *Journal of Geophysical Research*, *113*, B07408. https://doi.org/10.1029/2007JB005319
Suzuki, W., Aoi, S., Sekiguchi, H., & Kunugi, T. (2011). Rupture process of the 2011 Tohoku-Oki mega-thrust earthquake (M9.0) inverted from strong-motion data. *Geophysical Research Letters*, *38*, L00G16. https://doi.org/10.1029/2011GL049136
Tajima, F., Mori, J., & Kennett, B. L. N. (2013). A review of the 2011 Tohoku-Oki earthquake (Mw 9.0): Large-scale rupture across heterogeneous plate coupling. *Tectonophysics*, *586*, 15–34.
Takagi, R., & Okada, T. (2012). Temporal change in shear velocity and polarization anisotropy related to the 2011 M9.0 Tohoku-Oki earthquake examined using KiK-net vertical array data. *Geophysical Research Letters*, *39*, L09310. https://doi.org/10.1029/2012GL051342
TenCate, J. A. (2011). Slow dynamics of Earth materials: An experimental overview. *Pure and Applied Geophysics*, *168*, 2211–2219.
Tselentis, G., & Danciu, L. (2008). Empirical relationships between modified Mercalli intensity and engineering ground-motion parameters in Greece. *Bulletin of the Seismological Society of America*, *98*(4), 1864–1875.
Vallée, M., Ampuero, J. P., Juhel, K., Bernard, P., Montagner, J.-P., & Barsuglia, M. (2017). Observations and modeling of the elastogravity signals preceding direct seismic waves. *Science*, *358*, 1164–1168.
Viens, L., & Denolle, M. A. (2019). Long-period ground motions from past and virtual megathrust earthquakes along the Nankai trough, Japan. *Bulletin of the Seismological Society of America*, *109*(4), 1312–1330.
Wald, D., Quitoriano, V., Heaton, T., & Kanamori, H. (1999). Relationships between peak ground acceleration, peak ground velocity and modified Mercalli intensity in California. *Earthquake Spectra*, *15*(3), 557–564.
Wang, M., Li, Q., Wang, F., Zhang, R., Wang, Y., Shi, H., et al. (2011). Far-field coseismic displacements associated with the 2011 Tohoku-oki earthquake in Japan observed by Global Positioning System. *Chinese Science Bulletin*, *56*(23), 2419–2424.
Wang, R., Schurr, B., Milkereit, C., Shao, Z., & Jin, M. (2011). An improved automatic scheme for empirical baseline correction of digital strong-motion records. *Bulletin of the Seismological Society of America*, *101*(5), 2029–2044.
Wei, S., Graves, R., Helmberger, D., Avouac, J.-P., & Jiang, J. (2012). Sources of shaking and flooding during the Tohoku-Oki earthquake: A mixture of rupture styles. *Earth and Planetary Science Letters*, *333*, 91–100.
Yaghmaei-Sabegh, S., Tsang, H.-H., & Lam, N. T. K. (2011). Conversion between peak ground motion parameters and modified Mercalli Intensity values. *Journal of Earthquake Engineering*, *15*, 1138–1155.
Yagi, Y., & Fukahata, Y. (2011). Rupture process of the 2011 Tohoku-Oki earthquake and absolute elastic strain release. *Geophysical Research Letters*, *38*, L19307. https://doi.org/10.1029/2011GL048701
Yamada, N., & Iwata, T. (2005). Long-period ground motion simulation in the Kinki area during the MJ 7.1 foreshock of the 2004 off the Kii peninsula earthquakes. *Earth Planets and Space*, *57*, 197–202.
Zahradník, J., & Plešinger, A. (2010). Toward understanding subtle instrumentation effects associated with weak seismic events in the near field. *Bulletin of the Seismological Society of America*, *100*(1), 59–73.

Zhao, B., Wang, W., Yang, S., Peng, M., Qiao, X., Du, R., & Nie, Z. (2012). Far field deformation analysis after the Mw9.0 Tohoku earthquake constrained by cGPS data. *Journal of Seismology*, *16*(2), 305–313.

Zhu, L. (2003). Recovering permanent displacements from seismic records of the June 9, 1994 Bolivia deep earthquake. *Geophysical Research Letters*, *30*(14), 1740. https://doi.org/10.1029/2003GL017302